ACTUATORS

Explosion-powered eversible tactile displays

Ronald H. Heisser[1]†‡, Khoi D. Ly[1]†, Ofek Peretz[1], Young S. Kim[1], Carlos A. Diaz-Ruiz[1], Rachel M. Miller[1], Cameron A. Aubin[1]§, Sadaf Sobhani[1], Nikolaos Bouklas[1,2], Robert F. Shepherd[1]*

High-resolution electronic tactile displays stand to transform haptics for remote machine operation, virtual reality, and digital information access for people who are blind or visually impaired. Yet, increasing the resolution of these displays requires increasing the number of individually addressable actuators while simultaneously reducing their total surface area, power consumption, and weight, challenges most evidently reflected in the dearth of affordable multiline braille displays. Blending principles from soft robotics, microfluidics, and nonlinear mechanics, we introduce a 10-dot–by–10-dot array of 2-millimeter-diameter, combustion-powered, eversible soft actuators that individually rise in 0.24 milliseconds to repeatably produce display patterns. Our rubber architecture is hermetically sealed and demonstrates resistance to liquid and dirt ingress. We demonstrate complete actuation cycles in an untethered tactile display prototype. Our platform technology extends the capabilities of tactile displays to environments that are inaccessible to traditional actuation modalities.

INTRODUCTION

The dream of communicating electronic information through the sense of touch is nearly as old as modern computing. Among the first tactile display attempts were Robert Gault's teletactor in 1933 (*1*), a device that attempted to spread the various frequencies in speech as vibrations across the palm for the deaf, and a "hearing glove" prototype that Norbert Wiener designed and demonstrated for Helen Keller in 1949 (*2*, *3*). The Optacon, a "seeing finger" for blind readers, directly converted images from a scanning stylus to vibration patterns in a 144-pin array connected to piezoelectric bimorph actuators, providing high-resolution tactile images of any printed text to one index finger (*4*, *5*). Although simple vibrotactile feedback mechanisms are now ubiquitous in mobile phones, game controllers, and laptop track pads, knowledge of the millions of touch receptors in our skin motivates modern platforms that poke and prod with the resolution of skin's spatial acuity over large surface areas. Design requirements for wearable, untethered haptic feedback devices add constraints to this endeavor; for example, an actuation surface must also conform to the body, resist dirt and moisture, and tolerate user wear and tear.

Here, we focus on the development of millimeter-scale tactile displays needed to modernize precision computer access for people who are blind or deafblind or have limited vision—a litmus test for high–degree-of-freedom (DoF) actuation arrays (we use "blind" generally here). The "Holy Braille" challenge outlines design requirements for a currently unrealized full-page refreshable braille e-reader (*6*, *7*). A full page of braille has 25 lines, each line having 40 braille cells that use combinations of six possible dots to form characters, totaling 6000 actuators in a refreshable display. Given the size of a page of braille, portable multiline braille displays will likely have fewer than 6000 dots, although no single design has been decided. Dots should rise ~1 mm in a sequence fast enough to refresh the entire display in 0.1 to 1 s, depending on the reading application (*6*).

Same as visual literacy, the ability to read braille words constructed from individual characters is crucial for cognitive fluency and strongly correlates with upward social mobility (*8*–*10*). Unlike computer screens, most commercially available braille displays have a single line of 40 characters or fewer; users who are blind can only read small snapshots of digital text at a time (see fig. S7A). The lack of progress in braille display technology has allowed for an increasing reliance on text-to-speech screen reading software that circumvents learning braille. Although convenient, the greater use of screen readers and the disincentivization of teaching braille in public school systems continue to lower global braille literacy. Therefore, multiline displays are essential for two reasons. First, they enable computer graphical unit interface interactions, such as editing spreadsheets, reading sheet music, and practicing mathematics and computer science. Second, these technologies promote the mastery of braille in an increasingly digital age. We provide additional contextual discussion in Supplementary Methods.

In the past 5 years, new commercial ventures have proposed untethered, portable multiline display solutions (fig. S7). For example, Dot Inc. has engineered a braille cell (a six-dot unit) of electromagnetic flip-latch actuators for use in their own multiline e-reader (Dot Pad, 2400 actuators) and kiosk (*11*, *12*). Tactile Engineering Inc. recently announced a handheld, four-line–by–12-cell device (Cadence, 384 actuators) that can wirelessly mate with additional devices to extend the reading range to eight lines of 24 cells (*13*). These actuation systems have fast refresh rates and scalable architectures yet suffer the drawbacks of tight manufacturing tolerances, high part counts, and high costs (see table S3). These systems are also sensitive to dirt accumulation, liquid ingress, and drop impact, requiring frequent maintenance because a single malfunctioning dot can render a cell or line useless.

The interdisciplinary field of soft robotics embraces diverse and unconventional modes of actuation, aiming to improve device size, weight, power consumption, and cost (SWaP-C) (*14*, *15*). Hallmark soft robotic devices rout pressurized air to inflate elastomeric chambers, producing mechanical work without sliding parts, and are naturally resistant to damage from impact, having potential to solve some elusive tactile display design challenges. However, valve-based control strategies have prohibitively low SWaP-C performance when valves are individually connected to actuators, given their bulk, power consumption,

[1]Department of Mechanical and Aerospace Engineering, Cornell University, Ithaca, NY 14850, USA. [2]Pasteur Labs, Brooklyn, NY 11205, USA.
*Corresponding author. Email: rfs247@cornell.edu
†These authors contributed equally to this work.
‡Present address: Department of Mechanical Engineering, Massachusetts Institute of Technology, Cambridge, MA 02139, USA.
§Present address: Robotics Department, University of Michigan, Ann Arbor, MI 48109, USA.

and cost (*16*). The benefits of haptic pneumatic actuation continue to motivate advances in microfluidic logic systems (*17*), including efforts from NewHaptics to build a pneumatic braille display (*18*). Recent electrofluidic soft actuation methods have been proposed for haptic arrays, including submillimeter-thick hydraulically amplified electrostatic soft actuators that can produce 1 mm of deformation in a 5-mm^2–by–5-mm^2 footprint and electro-osmotic actuators that can raise 2-mm-diameter dots to heights >1 mm in 1 s (*19*, *20*).

Here, we extend the operational capabilities of multiline tactile displays with an array of domed membranes that evert (turn inside out) upward by explosive pressure differentials and downward by vacuum suction. Previous work demonstrates that by spark-igniting microliter volumes of oxyfuel gas mixtures inside elastomeric chambers, arrays of fluidic actuators can be individually controlled without valves (*16*, *21*, *22*). By leveraging elastomeric bistability, we have produced a latching display platform that is hermetically sealed, has no sliding parts, and reduces the total moving part count from thousands to a single-molded sheet. Applied to tactile displays, our device architecture can bring affordable, large-format systems to environments (i.e., transit stations, the kitchen, or outdoor spaces) in which current displays cannot feasibly operate (*23*). We compare current technologies in Supplementary Methods and table S3.

RESULTS

Array design

Figure 1A shows our eversible tactile display, consisting of 100 equidistant dots arranged in a 10-dot by 10-dot pattern. Each dot has a 2-mm base diameter, is ~1-mm high, and is spaced 2.5-mm center-to-center from neighboring dots. Compression molding formed the arrayed actuation membrane from one-part high-consistency silicone rubber (Fig. 1A). The full array comprised three layers of molded polydimethylsiloxane (PDMS) stacked on a rigid printed circuit board (PCB) that we encapsulated in PDMS to form a compatible adhesion surface.

Each of the four nonactuating layers had microfluidic conduits that carried fuel and exhaust gas mixtures throughout the device (Fig. 1A, gas route). We organized these channels perfusively; they

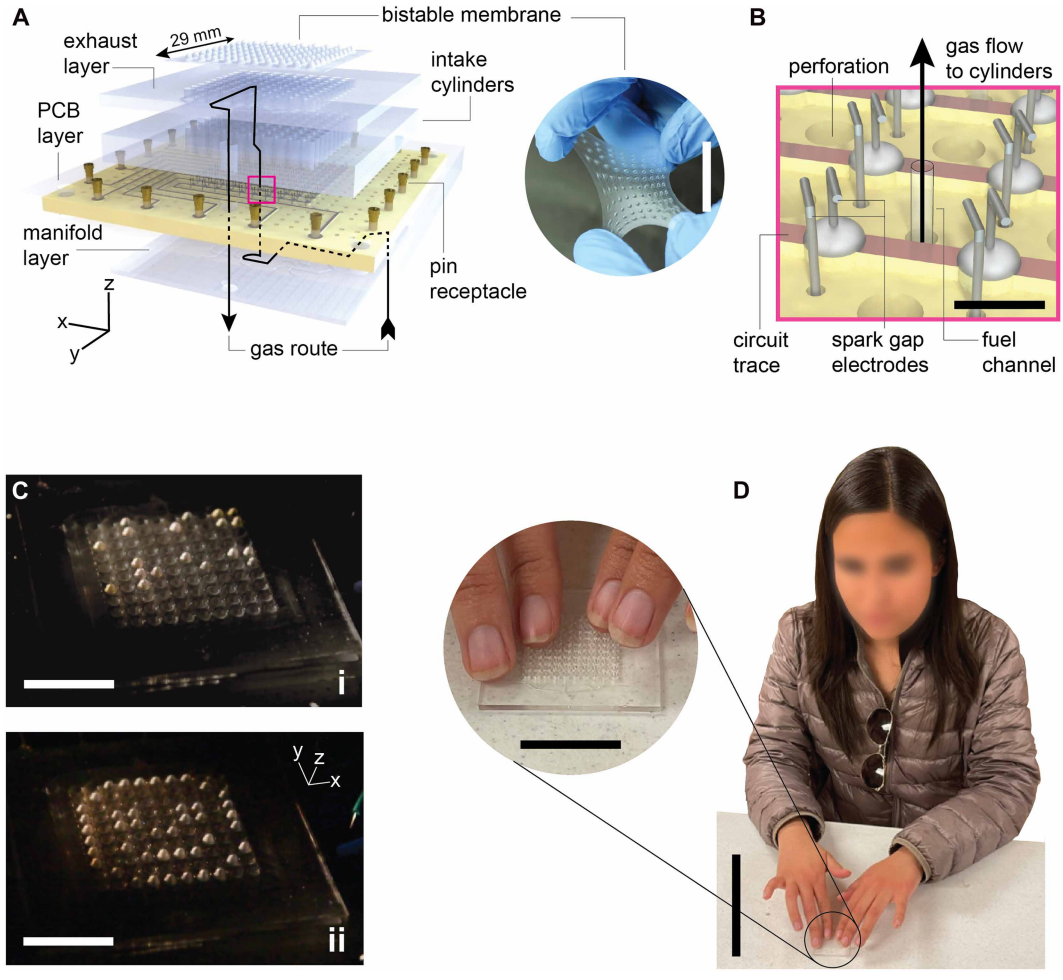

Fig. 1. Microcombustion generates legible tactile display patterns. (**A**) Stacked, molded PDMS layers efficiently distribute fuel and exhaust through actuator cylinders. The gas route goes through a single cylinder (three down, six across). Photo of membrane layer visualizing its hyperelasticity. Magenta square corresponds to design detail in (B). Scale bar, 25 mm. (**B**) Magnified rendering of PCB layer showing arrangement of electrodes bent and resting on top of the PDMS surface. Perforations mechanically engage cured PDMS with both sides of the PCB. Scale bar, 1.5 mm. (**C**) Display shows "Big Red" in uncontracted or grade 1 braille (i). Display shows smiling emoji with an included nose (ii). Scale bars, 15 mm. (**D**) A participant tests feel and legibility of the display surface. Scale bars, 125 mm (main image) and 25 mm (zoomed-in image).

three-dimensionally penetrated through the structure of the actuators, mimicking arterioles and venules that connect to form capillary networks (*24*). A single intake gas channel is connected to the bottom of the device, where oxygenated reactant gas entered and successively branched until it flowed upward through the PCB into one of the 100 possible combustion cylinders (Fig. 1B). After combustion, deoxygenated exhaust gas coalesced into one exhaust channel and exited the device, refreshing with new reactant gas.

Spark-gap ignition triggered combustion in each cylinder. Pin receptacles along the PCB border transmitted high-voltage (HV) signals to the cylinder through crisscrossing circuit traces. New silicon carbide opto-MOSFET (metal–oxide–semiconductor field–effect transistor) relays provided a compact means to switch HV signals as high as 3.3 kV from a single dc-dc converter (*16*). To generate a spark, one HV relay switched a top, widthwise (*x* direction Fig. 1A) trace to +V, and another relay switched a bottom, lengthwise trace to an HV-return or low-voltage (LV) line, generating a spark above from where the two traces intersected. Spark gaps were formed by soldering copper wires (40 American Wire Gauge, AWG) to pads on widthwise and lengthwise traces (Fig. 1B), given that they have simpler construction and greater wear resistance than microfabricated spark gaps (*25*). We left a portion of the wires protruding from the encapsulated PDMS surface to evenly space and laid them flat next to the cylinder intake port. Each igniter had an average gap distance of 87 ± 18 μm. We continuously switched sparks at 10 Hz for more than 200 hours and found no appreciable change in spark intensity or consistency. See Supplementary Methods and movies S1 to S3 for further manufacturing details.

We conducted initial pattern generation tests by connecting the device to an external HV control system and gas supply to sequentially ignite methane-oxygen mixtures with an equivalence ratio $\Phi = 0.34$. The equivalence ratio is a nondimensional relationship comparing the actual fuel-air (*F*/*A*) ratio with the stoichiometric *F*/*A*

$$\Phi = \frac{\left(\frac{F}{A}\right)_{\text{actual}}}{\left(\frac{F}{A}\right)_{\text{stoich}}} = \frac{\left(\frac{n_{\text{fuel}}}{n_{\text{air}}}\right)_{\text{actual}}}{\left(\frac{n_{\text{fuel}}}{n_{\text{air}}}\right)_{\text{stoich}}} \quad (1)$$

where *n* is the moles of the mixture species. Combining eversion with the kinetics of gas-phase combustion resulted in fast actuation speeds. High-speed videography showed that each dome flips upward in ~0.24 ms, having an average tip velocity of ~8.3 m s^{-1} (movie S4). Considering an average braille reading speed, devices need enough output power to facilitate ~1000 dot actuations per minute (*6*). During pattern generation, our system drew only 2.2 W from the HV amplifier and a pair of relays. We maintained consistent ignition performance at or below 30 Hz or 1800 actuations per minute, limited by switching times in the HV relays. Beyond this frequency, we found that misfiring occurs. Given that the relays we used have a specified total switching cycle time of ~1 ms, we believe that pattern generation rates can be improved to reduce the display refresh rate. Tactile displays have highly variable refresh rates that depend on the rising speed of each dot, aggregate dot power draw, and control sequences of onboard driving electronics. We defined refresh rate by the time taken to go from one static complete pattern to the next. Refresh rates in our system are limited by gas mixing and refilling times, discussed further in the "Untethered system integration" section.

As seen in Fig. 1C and movie S5, our array repeatably produced prescribed display states. Figure 1Ci shows a braille inscription of "Big Red." Figure 1Cii shows the ability to form tactile graphics, making a smile emoji. Once raised, the dots resisted downward eversion from finger pressure (movie S4). Pushing the dot to the surface of the tactile display with the finger did not displace the membrane to its critical buckling point, and the dot rose back to its raised position when the finger was lifted. We tested pressing forces of up to 35 N with a 9-mm-diameter post, and dots remained raised throughout (fig. S8). Further, we demonstrated some of the environmental advantages of our device's soft robotic design by pouring water on the display as a hexagonal pattern formed. The dots even splashed water out of the way as they rose (movie S6).

In our search of prior art, we could not find previous displays made of rubber. Therefore, we confirmed that our rubber displays tactile comfort and legibility by evaluating prescribed text patterns with nine braille readers. Participants had variable braille-reading experiences from years to 3 weeks. With our equidistant dot spacing (different from standard braille spacing), eight of the nine participants successfully read "Big Red." Advanced braille readers could quickly recognize the smile emoji.

Actuator mechanics

Core to our design is a thin, elastomeric membrane that everts from a concave pit to a convex dome. Our mold produced the convex geometry, so the initial configuration is the convex (upward) state. The dome is thimble shaped, having a variable thickness from 125 μm at its flexural hinge to 180 μm at its top, and is ~1 mm tall (Fig. 2A). The thickness variability is a unique control that can allow desirable actuation performance through design geometry optimization. Our design balances tactile legibility, manufacturing ease, and stability in the two everted states. Decades of research have explored the buckling, wrinkling, and snap-through instabilities of elastic shell structures, often focusing on spherical and ellipsoidal geometries. For a thin spherical cap, bistability depends on a relationship between the bending and stretching stresses along the membrane, being independent of material elasticity. Mechanicians typically represent this relationship with λ (*26*, *27*)

$$\lambda = \sqrt[4]{12(1-\nu^2)}\sqrt{\frac{R}{t}}\alpha \quad (2)$$

where ν, R, t, and α, respectively, represent Poisson's ratio, radius of curvature, thickness, and planar angle. Although this analysis is limited to spherical, constant thickness geometries, the formula provides intuition for our design effort. Previous experimental work demonstrated that free boundary condition (BC) "deep" shells with a curvature approaching a half sphere or $\alpha \lesssim 75°$ reliably exhibit bistable behavior for $\lambda > 5.75$. A 100-μm-thick spherical cap with a 2-mm base diameter and a 1-mm radius of curvature has $\lambda = 8.6$, comfortably bistable for the free case yet less so for our clamped BCs because of the added moment at the base (*28*).

Given a fixed thickness and base radius, taller ellipsoidal shells have higher axial stiffnesses than spherical shells (*29*, *30*). Therefore, our thimble-shaped braille dot could maintain a pronounced tactile feel without increasing the thickness, which would decrease eversion stability. It may also be possible to induce snap-through inversion at lower pressures by thoughtfully introducing membrane thickness variations or defects (*31*).

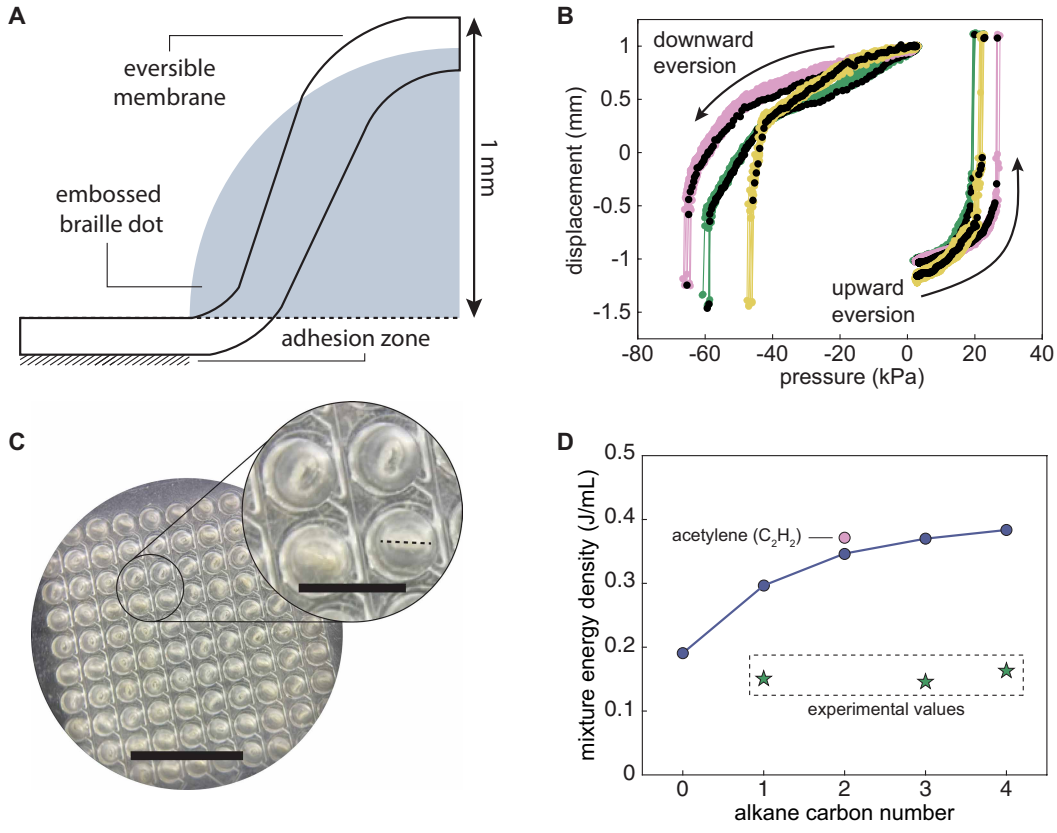

Fig. 2. Mechanical characteristics of a bistable braille dot. (**A**) Diagram compares membrane geometry cross section with maximum standard dimensions of embossed braille dot (in gray). The outer edge adheres to the lower PDMS layer on the bottom surface. (**B**) Experiments determine pressure-displacement relationships for individual membranes. The colored shaded areas are overlays of all points obtained during the eight measurements taken for each membrane sample, directly demonstrating low variability between individual actuation cycles. Each color represents a different membrane sample. The black dots show a single actuation cycle measurement for each membrane. (**C**) Image taken under the exhaust layer with downward-everted actuators. Inset shows exhaust channels. Dotted line shows leading edge of pinched duckbill shape. Scale bars, 10 mm and 2.5 mm (inset). (**D**) Points connected by the line show stoichiometric volumetric energy densities for oxyfuel mixtures of alkanes (C_nH_{2n+2}) that are gases at room temperature and pressure. We added acetylene to compare alkane energy densities with another commonly used premixed fuel. Green stars show energy densities for mixtures empirically determined to be compatible with our array system.

We experimentally characterized quasistatic downward and upward eversion by simultaneously measuring pressure and tip displacement while actuating the membrane with a syringe connected to a single chamber (Fig. 2B). Results showed that upward eversion requires, on average, ~20 kPa and downward eversion requires ~60 kPa of vacuum. If we assume a conservative estimated downward eversion pressure of 40 kPa (Fig. 2B) and a full 2-mm contact area, then the downward eversion pressure corresponds to a force of 125 mN, within previously described holding force limits of 50 mN (*6*). Critical membrane positions occurred near the dot surface (0 mm) for upward eversion and 0.5 to 0.75 mm under the dot surface for downward eversion. Thickness variability in membrane manufacturing influenced the snap-through critical load, especially when flipping downward. Finite element simulations suggested that our molding methods maintained membrane thickness deviations within 50 μm of the intended design (fig. S2). Downward-everted actuators tended to pinch into a duckbill shape, losing their upwardly axisymmetric form (Fig. 2C). Dots must resist snap-through from downward presses to be useful as a tactile reading surface. Fingers are generally not slender enough to push dots past the critical position, guaranteeing that a pattern will remain under normal operation until vacuum reset. Movie S6 shows that our actuators remain upright against different degrees of finger pressure despite being momentarily collapsible.

During actuation, pressure rise from combustion and membrane elasticity contribute to braille dot dynamics. Fingers that remain on a display as it refreshes will obstruct the motion of the moving dots. The microliter combustion volume and submilligram mass of each actuator's membrane amount to a brief, barely perceptible sensation on a fingertip. From video data, we estimated a membrane kinetic energy of 8 μJ compared with that of a stinging airsoft ball bearing, which can be more than 0.8 J (*32*). When slowly pressurized, rising dots critically buckle when the membrane center is within 0.1 mm of the display surface. Combustion introduces additional nonlinearities into the membrane's displacement. High-speed video reveals that when combustion-actuated membranes collide with an obstruction up to 0.9 mm above the display surface, they briefly remain in place and then suddenly flip back downward (Supplementary Methods). Given that an actuator stably crosses the critical buckling point under quasistatic conditions, further investigation will determine how combustion can be tuned to produce stable actuations under obstruction.

Although the actuator itself does no external work, we can still define efficiency with a minimum actuation energy (MAE) or the minimum energy required to induce upward eversion. To the first order, we estimated an average MAE of ~100 μJ from our experiments by calculating the pressure-volume work done on the membrane until it everted upward. Testing methane, propane, and butane, we determined oxyfuel stoichiometries that provided sufficient pressures to meet the MAE for our 2-mm-diameter, 7-mm-height actuator cylinder geometry (Fig. 2D). In our microliter combustion system, flames became unstable outside a range of intermediate fuel concentrations. Low fuel concentrations resulted in quenched flames, and high fuel concentrations caused flames energetic enough to propagate backward (flashback) through the microfluidic channels and ignite other chambers. We also established flashback and flame-quenching limits for each fuel in our actuator geometry (table S2). Oxymethane-powered eversions at $\Phi = 0.34$ had a chemomechanical efficiency of 0.086%. Operational propane ($\Phi = 0.35$) and butane ($\Phi = 0.33$) mixtures had efficiencies of 0.076 and 0.078%, respectively. In our system, combustion was naturally less efficient; open channels, low wall temperature, and high surface-to-area ratio all contributed to energetic losses at microliter scales (*16*, *33*). Considering mixture volumetric energy density and the required equipment for our fuel candidates, we believe that butane best suits this application.

Untethered system integration

We untethered our actuation system by integrating all functional components required for repeated display pattern generation onto an acrylic board. Figure 3A presents a system diagram of the main functional components (see Supplementary Methods and fig. S3 for system component details). An Arduino Mega controlled all relays, valves, and the vacuum pump. We programmed three buttons to execute the fuel intake, combustion, and vacuum steps of a display cycle (Fig. 3, B to D, respectively).

We connected butane and oxygen canisters to miniature gas regulators to make them compatible with the inline solenoid valves. The pressure regulator also reduced inline butane pressure below the room-temperature boiling point to ensure that only gaseous butane proceeded, given that small changes in butane stoichiometry can easily cross flashback and flammability limits at these length scales (*16*). The size and number of combustion chambers in our device require that gases be premixed before fuel intake. We accomplished this task simply by introducing a 3D printed elastomeric mixing chamber manifold connecting butane, oxygen, and fuel intake lines with integrated solenoid valves (Fig. 3B). The oxygen valve opened first, inflating a flat circular membrane until it reached a $\Delta p_{mix} = 5.3$ kPa set point (movie S7), measured by an onboard pressure sensor connected to the chamber. Then, the butane valve opened for 16 ms to mix in the fuel. Opening the third valve caused the membrane to deflate from its own hyperelasticity, filling the actuator array with new reactant gas and expelling the remaining exhaust gas through a check valve. Further, deflating the membrane ensured that no combustible amount of gas remained in the mixing chamber.

After combustion and tactile pattern generation, dots reset via a separate three-way valve that connects the vacuum chamber directly to the cylinder array. A portable diaphragm pump first pulled air from a 50-ml conical tube until reaching a gauge pressure of $\Delta p_{vac} = -62$ kPag (Fig. 3D). Powering the valve connected the array to the vacuum chamber and flipped all dots downward, causing the soft array to slightly "pucker" inward (movie S7). Excluding membrane and fluid dynamics, the pressure required to pull the dots back down can be expressed by the following relationship

$$p_{vac} = \frac{V_{ch} + V_{ar}}{V_{ch}} \left(p_{st} - p_{amb} \frac{V_{ar}}{V_{ch} + V_{ar}} \right) \quad (3)$$

where V_{ch} is the vacuum chamber volume, V_{ar} is the actuator array volume, p_{st} is the membrane downward snap-through pressure, and p_{amb} is the ambient pressure. We calculated $p_{vac} = -63.5$ kPag when assuming $p_{st} = -60$ kPag, close to our measured vacuum set point. Given that the system's exhaust port check valve prevents backflow of ambient air, the actuator array remained at a negative gauge pressure, and new gas re-established ambient pressure; the pressure differential helped pump fresh reactant into the array faster than just with the mixing chamber membrane's own elasticity. Once gas had replenished the array, the next actuation sequence could occur.

Compared with conventional electromechanical strategies, our combustion-powered display refresh cycles had additional steps to process fuels. Our current untethered display prototype is oxygen-limited in its capacity. Accounting for additional reactant gas in the external fuel channels, we conservatively assumed that a refresh volume twice the volume of the actuator can refill the display. Then, our 18-ml butane canister had enough fuel for almost 20,000 refreshes, whereas our 5-liter oxygen canister carried 1200 refreshes worth of gas.

The combined time for mixing and filling (20 s), pattern generation (3 s), and vacuum reset (1.5 s) was 24.5 s (movie S7). The mixing and refilling step is slow at present because of our simple elastomeric mixing chamber. We can reduce this time by directly injecting needed quantities of butane in line with a pressurized oxygen stream. By matching oxygen pressure to the 243-kPa vapor pressure of liquid butane at room temperature, we can achieve flow rates greater than 10 ml s^{-1} in our microfluidic channel geometries. Given that the total volume of all 100 actuators in our system is 2.2 ml, we believe that these flow rates can refill our current system in under 1 s. Our tethered experimental setup produced reactant flow rates of 2 ml s^{-1} and enabled >1-Hz combustion in single actuators. Figure S9 contains additional discussion of how refreshing processes can run in parallel to be compatible with braille reading times, especially for large-format braille displays.

DISCUSSION

We have developed a soft, scalable actuation array system that repeatably produces latched display states at the braille scale. Our simple architecture of spark gap electrodes, microfluidic channels, and eversible elastomeric membranes enables massive moving part reduction and thereby lowers material cost and manufacturing complexity, scaling to an arbitrary number of actuators. For $2n$ row-column pairs, the total HV relay area scales as $A_{relay} \sim n$ and the dot area scales as $A_{dot} \sim n^2$. For our unit relay area, the two footprints reach parity after 18 rows. For our design, a full page of braille needs 155 relays; relays occupy a fraction of the page area (Fig. 3E and fig. S3). Therefore, the components required to control actuation can fit neatly under the actuation surface for larger reading formats.

Our prototype system mechanically resets dots through vacuum and replenishes gas in each chamber to refresh the display with a new pattern. The added fuel steps currently result in a lower refresh rate for our device than other systems on the market; given longer instances of reading for scaled display systems, fast refresh rates are a less critical device metric. We believe that this drawback is worth

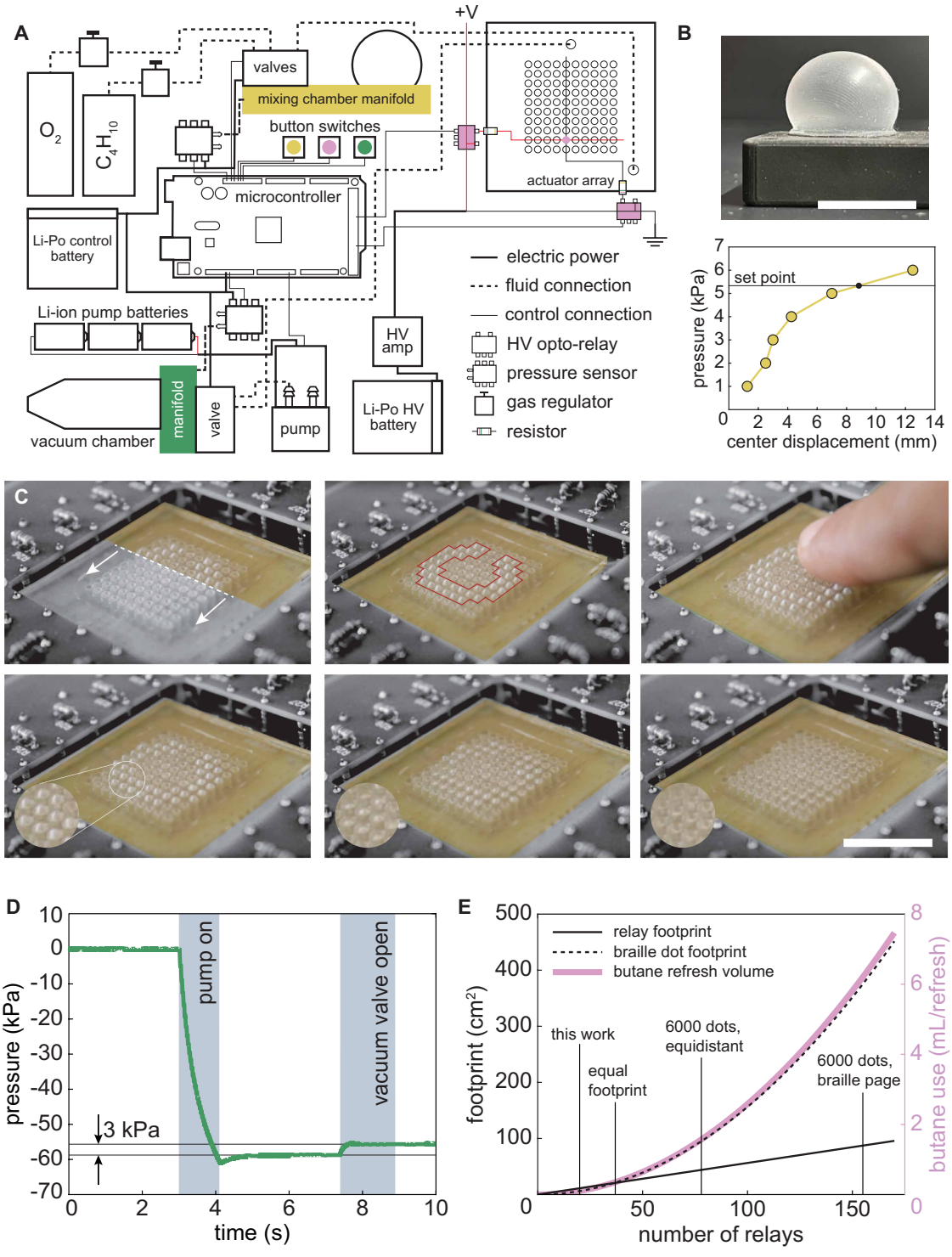

Fig. 3. Untethered tactile display operation. (**A**) Simple electrical and fluidic components connect to perform fuel intake, pattern generation, and vacuum reset actions. (**B**) The elastomeric mixing chamber inflates with oxygen until reaching a pressure set point and then receives a metered volume of butane gas, pumping the mixture when the intake valve is opened. Scale bar, 15 mm. (**C**) A large, bold "C" forms on the tactile display and resets after reading. The actuator array plugs into the system from under the PCB (gold pins). Scale bar, 20 mm. (**D**) Plot shows vacuum chamber pressure over a single-array reset. After initial vacuum establishment, the pump only needs to restore ~3 kPa per display cycle. (**E**) Many actuation strategies have repeated control components that scale incompatibly with the size of the overall device. Although the total area of 20 relays is larger than our 10-dot–by–10-dot display, the HV control relays would have a smaller footprint than the actuators after only 38 relays, or 361 dots, are used. A full page of braille is 816 cm^2, including margins, and would require 155 relays, which occupies 87 cm^2.

exploring further, given the system advantages of our soft, fluidic framework. The display surface is sealed from the external environment and can operate in wet, dirty environments that risk failure in current displays. For example, we envision a desktop implementation of our device useful for reading recipes while cooking, where oil and ingredients would not cause dot jamming in our membranes. The surface can be wiped clean or washed with soap and water. As a kiosk, our display could provide valuable information in unpredictable public spaces such as museums, libraries, and convention centers. Outside, our device can operate through rain, dirt, and pollution at parks and bus stops.

Tactile displays require maintenance from dot failure during use. Most display systems are highly integrated and must be shipped for professional repairs, historically leaving users without digital braille access for weeks at a time. Because our display connects simply to the other system components from press-fit gas connections and electrical contacts, no formal training is required to install a new display. We take less than 30 s to replace the 10-dot–by–10-dot array in our prototype.

Our untethered system contains all necessary components to repeatedly produce tactile patterns. Given the nature of components needed to supply fuel and pull vacuum, this system is unlikely to have the slim profile of a typical e-reader. The need for a stored source of oxygen is the core limitation of this technology because it has a lower density than the liquid butane fuel and will need more frequent replacement. Oxygen concentrators that normally supply >5 liters min^{-1} for breathing could be miniaturized to supply the milliliter min^{-1} gas consumption requirements for this system. The recent severe acute respiratory syndrome coronavirus 2 (SARS-CoV-2) pandemic has inspired research into compact electrochemical oxygen generators that could be modified to fit our system's oxygen requirements (*34*). The scale and brevity of combustion needed in our system warrant an investigation into other recyclable chemical actuation strategies such as water electrolysis–generated hydrogen combustion, ultraviolet photocatalysis of electrolyzed conjugate base pairs, and the controlled decomposition of hydrogen peroxide (*35*, *36*).

The most expensive component in this display is the HV relay. At our low-volume cost of $40 per relay, a full page of braille would require $6200 of these components (see fig. S5 for the materials cost of this prototype). We generate sparks at 2 kV, although we observed sparks at voltages as low as 1.2 kV. With more precise alignment of electrodes, we believe that we can use 1.5-kV relays, which have unit costs of under $5 at scale (see Panasonic AQV258). Figure S5 contains a material cost breakdown of our prototype.

Our system has potential to scale to thousands of actuators and serve applications beyond tactile displays. Designers can integrate bistable domes into other microfluidic systems to improve mechanical capabilities of droplet production and other manufacturing processes (*37*, *38*). High-throughput cell processing equipment could benefit from large arrays of pumps, valves, or microwell agitators (*39*). With our general actuation framework, high-density arrays of combustion cylinders could couple to cell substrates such that finely tuned pulses apply small strains to the cells, enhancing cell proliferation, alignment, and biochemical production (*40*–*42*).

MATERIALS AND METHODS

Device fabrication

We cured individual layers of PDMS using 3D printed molds to form the intake and exhaust channels and combustion cylinders. The electrode layer with out-of-plane channels was a perforated PCB encapsulated in PDMS to provide a compatible bonding surface with the other actuator layers. Each PDMS layer used 50 μm of prepolymer as adhesive. Eversible actuator sheets were hot-press molded out of one-part silicone (high-consistency rubber, Elastosil 4001/40 MH, Wacker) using a custom-machined aluminum mold and were bonded to the top of the device with a 25-μm layer of silicone epoxy (Sil-Poxy, Smooth-On).

The system prototype combined off-the-shelf and custom components onto a single laser-cut acrylic sheet to visualize all system parts with their fluidic and electric connections. The female pins lining the edge of the actuator array were connected to opposing pins on a system PCB. We fastened the corners of the actuator to the acrylic board to ensure connection. Separate onboard batteries powered the electronic control system, HV electronic components, and vacuum pump. The 3D printed mixing chamber and vacuum chamber had integrated channels that are connected to the solenoid valves. The 3D printed scaffolds held the oxygen and butane canisters in the depressed position for downstream valve flow control.

Pressure-displacement test

We obtained the pressure-displacement relationship of our bistable actuator by simultaneously measuring the membrane position and chamber pressure through eversion and inversion cycles, manually controlling pressure for the experiments. We bonded a single membrane to an isolated chamber, connected the intake port to a syringe, and connected the exhaust port to a piezoresistive pressure sensor (SSCDRRN015PDAA5, Honeywell). Above the membrane is a laser displacement sensor aligned with the membrane's center. We took measurements by slowly pushing the syringe depressor until the membrane flipped up and pulling the depressor until the membrane flipped down.

Fuel test

Using the actuator array, we empirically determined operational oxyfuel stoichiometries by varying the reactant flow rate and igniting a single dot until successful latching occurred. Mass flow controllers (MFCs) maintained flow rates with a precision of 0.1 ml min^{-1}. We used a laboratory compressed gas cylinder for methane experiments. We connected a butane canister to a water column to filter out butane steam that caused stoichiometry errors. We connected a miniature propane tank to a gas grill regulator to match operating pressures with the MFCs.

Pattern formation test

We conducted initial actuator array tests with our tethered experimental setup using methane for simplicity. Each HV trace is connected to an HV relay through PCB wires connected to a breadboard. Arduino protocols controlled the ignition sequences.

Untethered system actuation cycle test

The untethered system components were arranged in an exploded assembly format on an acrylic sheet to make all parts visible. Three separate batteries isolated the HV electronics, control electronics, and vacuum pump. A PCB was custom-designed to combine the microcontroller and HV components into one component that connected to the actuator array. To test the entire system, a display pattern was loaded onto the Arduino, and three input buttons were programmed to initiate fuel mixing and intake, ignition sequences, and

vacuum reset. Onboard oxygen (10 liters of Natural, Boost Oxygen) and butane (75 ml of butane fuel, Ronson) connected via miniature pressure regulators (3834 T51, McMaster-Carr) to two-way solenoid valves (X-8-05-S-F, Parker-Hannifin) provided the necessary oxyfuel mixture species, with volume control given by the pressure sensor. After filling, the combustion sequence initiated and produced the desired tactile pattern. Then, the vacuum chamber was set to the appropriate negative gauge pressure, and the dots were reset when pressing the final input button.

Supplementary Materials

The PDF file includes:
Methods
Figs. S1 to S9
Tables S1 to S3
Legends for movies S1 to S7
References (*43*)

Other Supplementary Material for this manuscript includes the following:
Movies S1 to S7
MDAR Reproducibility Checklist

REFERENCES AND NOTES

1. R. H. Gault, L. D. Goodfellow, Eliminating hearing in experiments on tactual reception of speech. *J. Gen. Psychol.* **9**, 223–228 (1933).
2. N. Wiener, Problems of sensory prosthesis. *Bull. Am. Math. Soc.* **57**, 27–35 (1951).
3. M. Mills, On disability and cybernetics: Helen Keller, Norbert Wiener, and the hearing glove. *differences* **22**, 74–111 (2011).
4. N. Efron, Optacon—a replacement for braille? *Aust. J. Optom.* **60**, 118–129 (1977).
5. L. H. Goldfish, H. E. Taylor, The optacon: A valuable device for blind persons. *J. Vis. Impair. Blind.* **68,** 49–56 (1974).
6. N. Runyan, D. Blazie, "EAP actuators aid the quest for the 'Holy Braille' of tactile displays" in *Electroactive Polymer Actuators and Devices* (*EAPAD*) *2010* (SPIE, 2010), vol. 7642, p. 764207; https://www.spiedigitallibrary.org/conference-proceedings-of-spie/7642/764207/EAP-actuators-aid-the-quest-for-the-Holy-Braille-of/10.1117/12.847764.short.
7. A. Russomanno, S. O'Modhrain, R. B. Gillespie, M. W. M. Rodger, Refreshing refreshable braille displays. *IEEE Trans. Haptics* **8**, 287–297 (2015).
8. A. M. Silverman, E. C. Bell, The association between braille reading history and well-being for blind adults. *J. Blind. Innov. Res.* **8**, 10.5241/8-141 (2018).
9. E. C. Bell, A. M. Silverman, Rehabilitation and employment outcomes for adults who are blind or visually impaired: An updated report. *J. Blind. Innov. Res.* **7**, 10.5241/8-148 (2018).
10. R. Ryles, The impact of braille reading skills on employment, income, education, and reading habits. *J. Vis. Impair. Blind.* **90**, 219–226 (1996).
11. Dot Inc.; http://www.dotincorp.com/.
12. J. Kim, B.-K. Han, D. Pyo, S. Ryu, H. Kim, D.-S. Kwon, Braille display for portable device using flip-latch structured electromagnetic actuator. *IEEE Trans. Haptics* **13**, 59–65 (2020).
13. Tactile Engineering; https://tactile-engineering.com.
14. Y. Jung, K. Kwon, J. Lee, S. H. Ko, Untethered soft actuators for soft standalone robotics. *Nat. Commun.* **15**, 3510 (2024).
15. C. A. Aubin, B. Gorissen, E. Milana, P. R. Buskohl, N. Lazarus, G. A. Slipher, C. Keplinger, J. Bongard, F. Iida, J. A. Lewis, R. F. Shepherd, Towards enduring autonomous robots via embodied energy. *Nature* **602**, 393–402 (2022).
16. R. H. Heisser, C. A. Aubin, O. Peretz, N. Kincaid, H. S. An, E. M. Fisher, S. Sobhani, P. Pepiot, A. D. Gat, R. F. Shepherd, Valveless microliter combustion for densely packed arrays of powerful soft actuators. *Proc. Natl. Acad. Sci. U.S.A.* **118**, e2106553118 (2021).
17. A. A. Stanley, E. S. Roby, S. J. Keller, High-speed fluidic processing circuits for dynamic control of haptic and robotic systems. *Sci. Adv.* **10**, eadl3014 (2024).
18. NewHaptics; https://www.newhaptics.com/.
19. A. Firouzeh, A. Mizutani, J. Groten, M. Zirkl, H. Shea, PopTouch: A submillimeter thick dynamically reconfigured haptic interface with pressable buttons. *Adv. Mater.* **36**, e2307636 (2024).
20. V. Shen, T. Rae-Grant, J. Mullenbach, C. Harrison, C. Shultz, "Fluid reality: High-resolution, untethered haptic gloves using electroosmotic pump arrays" in *Proceedings of the 36th Annual ACM Symposium on User Interface Software and Technology* (Association for Computing Machinery, 2023), pp. 1–20.
21. C. A. Aubin, R. H. Heisser, O. Peretz, J. Timko, J. Lo, E. F. Helbling, S. Sobhani, A. D. Gat, R. F. Shepherd, Powerful, soft combustion actuators for insect-scale robots. *Science* **381**, 1212–1217 (2023).
22. D. P. Holmes, A. J. Crosby, Snapping surfaces. *Adv. Mater.* **19**, 3589–3593 (2007).
23. P. M. Reis, A perspective on the revival of structural (in)stability with novel opportunities for function: From buckliphobia to buckliphilia. *J. Appl. Mech.* **82**, 111001 (2015).
24. J. A. E. Spaan, "Structure and perfusion of the capillary bed" in *Coronary Blood Flow: Mechanics, Distribution, and Control*, J. A. E. Spaan, Ed. (Springer, 1991), pp. 69–86.
25. P. Seriburi, D. Kercher, M. G. Allen, An experimental study of microfabricated spark gaps: Wear and erosion characteristics. *J. Micromech. Microeng.* **11**, 165–174 (2001).
26. M. Taffetani, X. Jiang, D. P. Holmes, D. Vella, Static bistability of spherical caps. *Proc. R. Soc. A Math. Phys. Eng. Sci.* **474**, 20170910 (2018).
27. J. R. Fitch, The buckling and post-buckling behavior of spherical caps under concentrated load. *Int. J. Solids Struct.* **4**, 421–446 (1968).
28. P. M. Sobota, K. A. Seffen, Effects of boundary conditions on bistable behaviour in axisymmetrical shallow shells. *Proc. R. Soc. A.* **473**, 20170230.
29. A. Lazarus, H. C. B. Florijn, P. M. Reis, Geometry-induced rigidity in nonspherical pressurized elastic shells. *Phys. Rev. Lett.* **109**, 144301 (2012).
30. D. Vella, A. Ajdari, A. Vaziri, A. Boudaoud, Indentation of ellipsoidal and cylindrical elastic shells. *Phys. Rev. Lett.* **109**, 144302 (2012).
31. J. W. Hutchinson, Buckling of spherical shells revisited. *Proc. R. Soc. A Math. Phys. Eng. Sci.* **472**, 20160577 (2016).
32. C. Grocock, R. McCarthy, D. Williams, Ball bearing (BB) guns, ease of purchase and potential for significant injury. *Ann. R. Coll. Surg. Engl.* **88**, 402–404 (2006).
33. E. Sher, I. Sher, Theoretical limits of scal announced a handheld ing-down internal combustion engines. *Chem. Eng. Sci.* **66**, 260–267 (2011).
34. Y. Zhang, K. Xie, F. Zhou, F. Wang, Q. Xu, J. Hu, H. Ding, P. Li, Y. Tan, D. Li, J. Zhu, H. Zhou, C. Zhao, S. Lin, Y. Wu, Electrochemical oxygen generator with 99.9% oxygen purity and high energy efficiency. *Adv. Energy Mater.* **12**, 2201027 (2022).
35. L. M. Egolf, J. T. Keiser, Photon-initiated hydrogen-chlorine reaction: A student experiment at the microscale level. *J. Chem. Educ.* **70**, A208 (1993).
36. M. Adami, A. Seibel, On-board pneumatic pressure generation methods for soft robotics applications. *Actuators* **8**, 2 (2018).
37. S. Battat, D. A. Weitz, G. M. Whitesides, An outlook on microfluidics: The promise and the challenge. *Lab Chip* **22**, 530–536 (2022).
38. M. Duran, A. Serrano, A. Nikulin, J.-L. Dauvergne, L. Derzsi, E. Palomo del Barrio, Microcapsule production by droplet microfluidics: A review from the material science approach. *Mater. Des.* **223**, 111230 (2022).
39. P.-Y. Gires, M. Thampi, M. Weiss, Miniaturized magnetic stir bars for controlled agitation of aqueous microdroplets. *Sci. Rep.* **10**, 10911 (2020).
40. C. L. Thompson, S. Fu, H. K. Heywood, M. M. Knight, S. D. Thorpe, Mechanical stimulation: A crucial element of organ-on-chip models. *Front. Bioeng. Biotechnol.* **8**, 602646 (2020).
41. A. Wahlsten, D. Rütsche, M. Nanni, C. Giampietro, T. Biedermann, E. Reichmann, E. Mazza, Mechanical stimulation induces rapid fibroblast proliferation and accelerates the early maturation of human skin substitutes. *Biomaterials* **273**, 120779 (2021).
42. B. Rios, A. Bu, T. Sheehan, H. Kobeissi, S. Kohli, K. Shah, E. Lejeune, R. Raman, Mechanically programming anisotropy in engineered muscle with actuating extracellular matrices. *Device* **1**, 100097 (2023).
43. T. Premkumar, "Braille display by rotating multi-octagonal segment" in *2017 Innovations in Power and Advanced Computing Technologies* (*i-PACT*) (IEEE, 2017), pp. 1–4.

Acknowledgments: We thank the Laboratory of Atomic and Solid State Physics (LASSP) Professional Machine Shop for experimental fabrication services. We thank the Carroll Center for the Blind and the Colorado Center of the Blind for display evaluation and discussions. We thank interviewees of the I-Corps program for myriad and fruitful discussions about braille and life experience. We thank N. Runyan for a lifetime of devotion to tactile display innovation and equity for the blind. **Funding:** This work was supported by the DOE Advanced Research Project Agency-Energy (ARPA-E) DE-AR0001855 (to R.F.S.), Office of Naval Research (ONR) N00014-20-1-2438 (to R.F.S.), and National Science Foundation (NSF) TI-2231592 (to R.F.S.). **Author contributions:** Conceptualization: R.H.H. and R.F.S. Methodology: R.H.H., K.D.L, O.P., C.A.D-R., C.A.A, S.S., N.B., Y.S.K., and R.F.S. Investigation: R.H.H., K.D.L, O.P., C.A.D.-R., R.M.M., C.A.A, S.S., N.B., Y.S.K., and R.F.S. Visualization: R.H.H., K.D.L., and R.M.M. Funding acquisition: R.F.S. Supervision: S.S., N.B., and R.F.S. Writing—original draft: R.H.H., K.D.L., O.P., and R.F.S. Writing—review and editing: R.H.H., K.D.L, O.P., C.A.A., S.S., N.B., and R.F.S. **Competing interests:** R.H.H., C.A.A., and R.F.S. are listed authors on US11353046B2. All other authors declare that they have no competing interests. **Data and materials availability:** Pressure-displacement data and control code for the untethered display are available for download on Dryad (https://doi.org/10.5061/dryad.70rxwdc9s).

Submitted 29 October 2024
Resubmitted 2 June 2025
Accepted 31 July 2025
Published 27 August 2025
10.1126/scirobotics.adu2381